Measurement and Assignment of Long-Range C−H Dipolar Couplings in Liquid Crystals by Two-Dimensional NMR Spectroscopy

Mei Hong and Alexander Pines*

Materials Sciences Division, Lawrence Berkeley National Laboratory, 1 Cyclotron Road, and Department of Chemistry, University of California, Berkeley, California 94720

Stefano Caldarelli

Section de Chimie de l'Université, BCH-Dorigny, CH-1015 Lausanne, Switzerland

Received: April 2, 1996; In Final Form: June 12, 1996[⊗]

We describe multidimensional NMR techniques to measure and assign $^{13}C-^{1}H$ dipolar couplings in nematic liquid crystals with high resolution. In particular, dipolar couplings between aromatic and aliphatic sites are extracted, providing valuable information on the structural correlations between these two components of thermotropic liquid crystal molecules. The NMR techniques are demonstrated on 4-pentyl-4′-biphenylcarbonitrile (5CB), a well-characterized room-temperature nematic liquid crystal. Proton-detected local-field NMR spectroscopy is employed to obtain highly resolved C−H dipolar couplings that are separated according to the chemical shifts of the carbon sites. Each ^{13}C cross section in the 2D spectra exhibits several doublet splittings, with the largest one resulting from the directly bonded C−H coupling. The smaller splittings originate from the long-range C−H dipolar couplings and can be assigned qualitatively by a chemical shift heteronuclear correlation (HETCOR) experiment. The HETCOR experiment incorporates a mixing period for proton spin diffusion to occur, so that maximal polarization transfer can be achieved between the unbonded ^{13}C and ^{1}H nuclei. To assign the long-range C−H couplings quantitatively, we combined these two techniques into a novel reduced-3D experiment, in which the ^{1}H chemical shift-displaced C−H dipolar couplings are correlated with the ^{13}C chemical shifts. The time domain of this experiment involves separate but synchronous incrementation of the evolution periods for the C−H dipolar couplings and the ^{1}H chemical shifts, with a variable ratio of the respective dwell times to optimize the resolution and facilitate resonance assignment in the spectrum.

Introduction

The physical properties of thermotropic liquid crystals are strongly dependent on their molecular shapes, a general feature of which is the presence of a rigid (often aromatic) core and a flexible (aliphatic) part.[1] Correlations between structural flexibility and orientational order in these molecules have been investigated by various NMR techniques exploiting anisotropic nuclear spin interactions.[2] On the basis of these studies, insight into the structure-orientation relation has been obtained and used to test molecular models for the nematic liquid crystals.[3−6] In NMR experiments, the dipolar interaction between the magnetic moments of two nuclei such as ^{13}C and ^{1}H provides a particularly sensitive probe of the variation in the segmental order and the conformational distributions in these mobile molecules.

An important NMR technique for determining $^{13}C-^{1}H$ dipolar couplings in nematic liquid crystals is two-dimensional (2D) separated-local-field (SLF) spectroscopy[7,8] in combination with variable-angle spinning of the liquid crystal.[9−12] In the separation of the C−H dipolar couplings according to the ^{13}C chemical shifts, the traditional SLF technique probes the anisotropic C−H dipolar local fields at the *carbon* sites. Because of the much higher number density of the ^{1}H nuclei, each ^{13}C nucleus is dipolar-coupled to several protons, which are either directly bonded or not bonded to it (i.e., short-range or long-range, respectively). Due to successive splittings, the SLF spectrum of a carbon coupled to N protons exhibits up to 2^N lines, even when homonuclear dipolar interaction among the protons is removed. The complexity of the SLF spectrum makes it difficult to extract the individual C−H dipolar couplings quantitatively, a particularly serious problem for long-range couplings that could provide important constraints on the structure and orientational order of liquid crystalline molecules.

In this paper, we present an alternative technique, based on proton-detected local-field (PDLF) NMR,[13−16] for determining both short-range and long-range C−H dipolar couplings. The PDLF technique yields high-resolution C−H couplings by probing (i.e., detecting) the dipolar local fields of the *proton* spins in the indirect dimension of the 2D experiment. Since each proton is usually coupled to only one ^{13}C spin due to the low (1.1%) natural abundance of ^{13}C, the PDLF spectrum exhibits one dipolar coupling pattern for each C−H spin pair, and a maximum of only $2N$ lines is observed for a ^{13}C spin coupled to N protons. The simplicity and the relatively high resolution of the PDLF spectrum allow the small long-range C−H couplings to be measured.

The dipolar coupling detection scheme (on ^{1}H's rather than ^{13}C's) of the PDLF technique and the simplicity of the resulting spectra also allow the identification of the ^{1}H coupling partners in C−H spin pairs. In the traditional carbon-detected SLF experiment, ^{1}H chemical shift frequencies are not measured. The assignment of a dipolar splitting to a C−H spin pair is usually based on ^{13}C chemical shifts and distance arguments. However, for dipolar couplings between two unbonded ^{13}C and ^{1}H nuclei in mobile molecules, this procedure fails because the magnitudes of the couplings are not known *a priori*. The assignment can be made if additional information on the ^{1}H

[⊗] Abstract published in *Advance ACS Abstracts,* August 1, 1996.

S0022-3654(96)00972-0 CCC: $12.00

chemical shift can be obtained. Indeed, a 3D experiment correlating the C−H dipolar coupling and the chemical shifts of both ^{13}C and ^{1}H sites can be expected to fulfill the requirement. However, ^{1}H chemical shifts cannot be obtained from a ^{13}C SLF 3D experiment because dipolar evolution of the ^{1}H spins is required to relate the ^{1}H chemical shifts with the observed C−H couplings. In contrast, the PDLF technique provides the necessary ^{1}H chemical shift information for identifying coupling partners in long-range C−H dipolar couplings.

To assign long-range C−H dipolar couplings, we combined a $^{13}C-^{1}H$ heteronuclear chemical shift correlation (HETCOR) experiment,[17,18] which provides qualitative evidence for the presence of heteronuclear dipolar couplings, with the PDLF experiment. Furthermore, we simplified this combination to produce a reduced-3D experiment, which is introduced and explained in this paper.

Caution must be exercised in the use of intense radio frequency (rf) fields for decoupling in the liquid crystalline phases, as the orientational order of these molecules can be very sensitive to the temperature gradients induced by high-power rf pulses. To avoid rf heating, we carried out the experiments under fast mechanical spinning of the sample, in analogy to the variable-angle spinning methodology used previously.[9,10] The magnitude of the dipolar coupling in the nematic phase depends on the angle β between the main symmetry axis (i.e., the director) of the phase and the magnetic field according to $P_2(\cos\beta) = {}^1/_2(3\cos^2\beta - 1)$.[12] In a nonspinning liquid crystal, the director is oriented by the magnetic torque to be either parallel or perpendicular to the magnetic field, depending on the sign of the anisotropy of the magnetic susceptibility $\Delta\chi$. In a rotating sample, however, the magnetic torque can be overcome by the viscous torque, causing the director to align instead with the spinning axis. A nematic phase with a positive $\Delta\chi$ can be oriented along the spinning axis when the spinning angle θ is smaller than the magic angle 54.7°.[11] Consequently, the dipolar coupling is reduced by a scaling factor $0 \leq P_2(\cos\theta) \leq 1$, and milder rf fields can be used for both homonuclear and heteronuclear dipolar decoupling.

In the following, we describe in detail the pulse sequences of the PDLF experiment, the chemical shift correlation experiment, and the reduced-3D experiment. We then demonstrate the structural information yielded by these techniques on room-temperature nematic phase 4-pentyl-4′-biphenylcarbonitrile, which has been previously characterized by NMR analysis of the ^{2}H quadrupolar couplings,[19] proton−proton[20,21] and carbon−proton dipolar couplings,[9] and ^{13}C chemical shift anisotropy.[22]

Experimental Section

The liquid crystal 4-pentyl-4′-biphenylcarbonitrile (5CB) was obtained from Aldrich Chemicals (Milwaukee, WI). The sample was placed in a 7 mm Doty (Columbia, SC) silicon nitride rotor, and the caps were glued to the rotor to prevent sample leakage. All NMR spectra were measured on a home-built 300 MHz spectrometer with a Tecmag pulse programmer and acquisition system. A home-built variable-angle spinning probehead was used.

The liquid crystal sample was spun at approximately 1.6 kHz about an axis inclined at an angle θ to the magnetic field. This spinning angle was controlled to within ±0.1° by a stepping motor attached to the bottom of the probe and a computerized motor controller.[23] Prior to each 2D experiment, the spinning angle was carefully referenced to the magic angle. The choice of the spinning angle θ or the scaling factor $P_2(\cos\theta)$ relies on two considerations. First, due to the positive anisotropic susceptibility ($\Delta\chi > 0$) of 5CB, θ must be smaller than the magic angle so that the nematic director aligns with the rotation axis.[11] Secondly, $P_2(\cos\theta)$ should be chosen to optimize the spectral resolution. If $P_2(\cos\theta)$ is too small, the long-range C−H dipolar couplings will barely be resolved. However, if it is too large, the low-power multiple-pulse decoupling may be insufficient to suppress the residual homonuclear couplings and the spectral resolution will deteriorate. We used a spinning angle of 50.7°, corresponding to a scaling factor of $P_2(\cos\theta) = +0.102$, for the experiments reported here.

The rf field strengths were set at a low level, usually between 33 and 38 kHz, to avoid overheating the sample. Typical ^{1}H and ^{13}C 90° pulse lengths were between 6.5 and 7.5 μs. The CP contact time was 2.5 ms in all experiments. The overall rf duty cycle ranged from 0.5% to 4%. The cycle time of the MREV-8 decoupling sequence[24,25] was usually between 110 and 130 μs. In the PDLF experiment, a maximum of 360 MREV-8 cycles was acquired in the evolution period. This corresponds to an effective evolution time of 20.3 ms or a dipolar coupling resolution of 16 Hz, assuming the theoretical MREV-8 scaling factor of 0.47.[24,25] The MREV-8 multiple-pulse sequence scales all effective interactions in the applied time period, including the C−H dipolar and scalar couplings and the ^{1}H chemical shifts. The chemical shift correlation experiment had a maximum evolution time of 256 MREV-8 cycles, giving a ^{1}H chemical shift resolution of about 24 Hz.

NMR Pulse Sequences. Figure 1a shows the pulse sequence for the C−H PDLF experiment. During the evolution period t_1, the ^{1}H magnetization evolves under the C−H dipolar and scalar (J) interactions. An MREV-8 multiple-pulse sequence[24,25] suppresses the H−H homonuclear interaction, and two simultaneous ^{1}H and ^{13}C 180° pulses in the middle of the t_1 period refocus the ^{1}H chemical shifts while retaining the C−H couplings. At the end of the evolution period, a ^{1}H spin-lock pulse of 1 ms selects the cosine-modulated dipolar coherence, which is then transferred to the carbon spins by Hartman−Hahn cross-polarization (CP).[26,27] During the t_2 period, the ^{13}C magnetization evolves under the chemical shift interaction and is detected in the presence of proton decoupling.

In all experiments the ^{1}H carrier frequency was kept the same and set within the ^{1}H spectral region, as the decoupling efficiency of the MREV-8 multiple-pulse sequence varies with the frequency offset. Improper setting of the ^{1}H carrier frequency could generate artificial splittings in the dipolar coupling dimension of the 2D spectrum. This possibility was eliminated by optimizing the MREV-8 performance with control experiments, whose pulse sequence is similar to that in Figure 1a but without the ^{1}H 180° pulse in the evolution period. As a result, the t_1 period becomes devoid of any effects of local NMR interactions, and the control spectrum should exhibit slow and smoothly decaying FIDs in t_1.

Since the proton carrier frequency is placed in the middle of the spectrum, both cosine- and sine-modulated frequencies would normally be required to discriminate the sign of the anisotropic couplings. However, due to the intrinsic symmetry of the dipolar spectra, the sine component of the dipolar coherence contains nearly vanishing signals and is time-consuming to acquire. Therefore, only the cosine-modulated dipolar coherence is detected, and the PDLF spectra are made symmetric in the ω_1 dimension.

The $^{13}C-^{1}H$ heteronuclear correlation experiment was conducted with the pulse sequence in Figure 1b. It involves ^{1}H chemical shift (CS) evolution, magnetization transfer from ^{1}H to ^{13}C through cross polarization, and detection of the ^{13}C chemical shifts. In the evolution period t_1, the MREV-8 sequence is again used to remove the H−H homonuclear couplings, whereas the ^{13}C 180° pulse refocuses the C−H

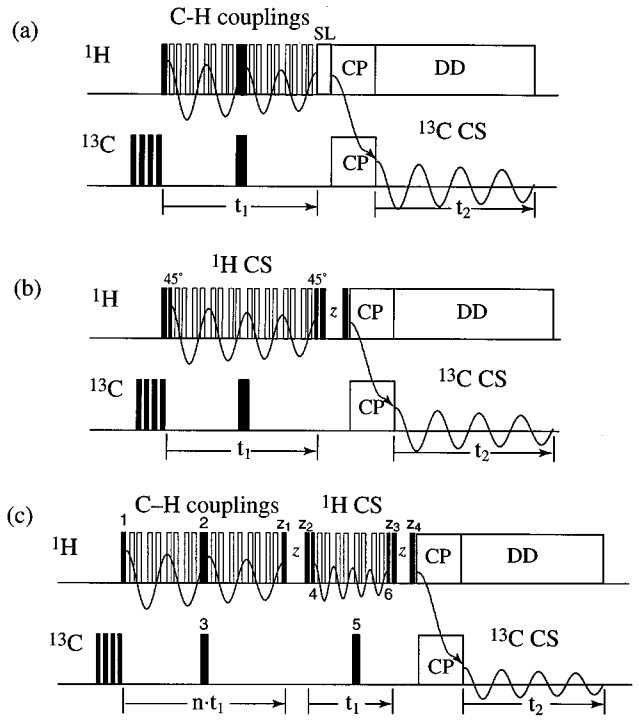

Figure 1. Pulse sequences of (a) the ^{13}C−^{1}H PDLF experiment, (b) the ^{13}C−^{1}H HETCOR experiment, and (c) the reduced-3D experiment. (a) In the evolution period t_1, ^{1}H magnetization evolves under the C−H dipolar and scalar interactions. The MREV-8 multiple-pulse sequence removes the H−H homonuclear couplings and a ^{1}H 180° pulse refocuses the ^{1}H chemical shifts. A ^{1}H spin−lock pulse selects the cosine-modulated dipolar coherence, which is then transferred to ^{13}C by cross-polarization. ^{13}C magnetization is detected during t_2 with proton decoupling. ^{13}C presaturation pulses are applied to ensure that only polarization resulting from ^{1}H is detected. (b) ^{1}H magnetization first evolves under the chemical shift interaction during the evolution period. Following a *z*-filter that selects the cosine- and sine-modulated frequencies separately, the ^{1}H magnetization is transferred to ^{13}C by CP and the ^{13}C chemical shifts are detected during t_2. The 45° pulses before and after the MREV-8 multiple-pulse train and the phase cycles of the ^{1}H pulses in t_1 serve to eliminate quadrature artifacts due to MREV-8. (c) Initially, ^{1}H magnetization evolves under C−H couplings in the same way as in the PDLF experiment. Then a 90° ^{1}H pulse stores cosine-modulated dipolar coherence along the *z*-axis for a short time (1 ms or less), after which the ^{1}H magnetization is flipped back to the *xy* plane of the rotating frame and evolves under the ^{1}H chemical shift interaction, in analogy to the HETCOR experiment. Subsequently, a second *z*-filter is applied and is followed by CP, after which the ^{13}C chemical shifts are detected. The States[28] acquisition method is employed for the ^{1}H chemical shifts. The PDLF and ^{1}H chemical shift evolution periods are incremented simultaneously to produce a reduced-3D spectrum. The dwell time ratio *n* is controlled by the relative number of MREV-8 cycles per increment.

couplings. At the end of the t_1 period, the cosine- and sine-modulated frequencies are recorded separately according to the States method[28] to obtain pure-phase ^{1}H chemical shift spectra. A *z*-filter before CP not only selects the desired frequency component but also can be extended to allow spin diffusion to occur among the protons. The latter allows the long-range C−H dipolar couplings to be detected with higher sensitivity.

The two ^{1}H 45°$_{\pm y}$ pulses[29] before and after the multiple-pulse train (Figure 1b) in the evolution period and the phase cycles of the ^{1}H pulses result from the adoption of the States detection scheme[28] and the MREV-8 effective field direction (1,0,1). The tilted effective field of MREV-8 causes the trajectory of the magnetization vector to deviate from the *xy* plane of the rotating frame. Thus, the acquired cosine and sine components of the chemical shift frequencies do not have the same magnitudes. As a result of this imbalance, a signal occuring at frequency $+\omega$ produces a quadrature image at the negative frequency $-\omega$.

TABLE 1: Phase Cycles Used in the Reduced-3D Experiment[a]

pulse	1	2	3,5	z_1	z_2	4	6	z_3	z_4	CPH	CPC	RC
phase	0	1	0	ρ	0	3	1	0	2	1	0, 1	$-\rho$
	2		0	ρ	2			0	2	1	0, 1	ρ
			1	ρ	1			1	3	2	0, 1	$-\lambda$
			1	ρ	3			1	3	2	0, 1	λ
			2	$-\rho$				2	0		2, 3	ρ
			2	$-\rho$				2	0		2, 3	$-\rho$
			3	$-\rho$				3	1		2, 3	λ
			3	$-\rho$				3	1		2, 3	$-\lambda$

[a] ρ = 2 0 2 0; $-\rho$ = 0 2 0 2; λ = 3 1 3 1; $-\lambda$ = 1 3 1 3; CPH = ^{1}H CP spin-lock; CPC, ^{13}C CP spin-lock; RC, receiver. z_1−z_4 are mixing pulses for the two *z*-filters. The z_3 phases shown here record the cosine component of the ^{1}H chemical shift. The sine component is detected by shifting the phases by 90°. The pulse nomenclature is indicated in Figure 1c.

This spurious quadrature image can be removed by a 45°$_y$ pulse applied immediately before the *z*-filter, since the pulse effectively rotates the precession plane perpendicular to the MREV-8 field axis to the *xy* plane of the rotating frame. However, since the precise duration of the 45° pulse is difficult to determine and the practical MREV-8 effective field direction may differ from the theoretical prediction, a fraction of the quadrature image might still remain. This potential artifact can be eliminated if the ^{1}H excitation pulse and the 90° pulse starting the *z*-filter are fully phase-cycled together with the receiver reference phase. To ensure that the initial magnetization created by the fully phase-cycled excitation pulse is always transverse to the MREV-8 effective field, another 45° pulse along $-y$ becomes necessary at the beginning of the t_1 period.

The combined PDLF and ^{1}H chemical shift experiment was carried out with the pulse sequence of Figure 1c. In the first time period, the ^{1}H magnetization evolves under the C−H interaction as in the normal PDLF experiment. A 90° pulse then stores the cosine-modulated dipolar coherence along the *z*-axis for 1 ms or less. Subsequently, the ^{1}H magnetization is flipped back to the transverse plane by the second 90° pulse and evolves under the chemical shift interaction in exactly the same way as in the HETCOR experiment (Figure 1b). The short *z*-filter between the two time periods enables the ^{1}H magnetization at the beginning of the chemical shift evolution to be fully phase-cycled, for the same reason as discussed above. After the ^{1}H chemical shift evolution, a second *z*-filter is applied to facilitate proton spin diffusion. Finally, the ^{1}H magnetization is transferred to ^{13}C by CP, and the ^{13}C chemical shifts are observed during the detection period. The detailed phase cycles for this reduced-3D pulse sequence are listed in Table 1.

The pulse sequence in Figure 1c consists of three distinct interaction periods, so that it would normally give rise to a 3D spectrum after Fourier transformation. However, the implementation of a 3D experiment is both instrumentally demanding and time-consuming. Therefore, we simplified this apparent 3D pulse sequence into a 2D version. The reduction in dimensionality is reminiscent of that of the "accordion" experiment.[30,31] The simplification is achieved by simultaneous incrementation of the first two time periods, which are dominated by the ^{1}H chemical shift and the C−H dipolar interactions. By this means, the two evolution periods are correlated and produce a single frequency dimension after Fourier transformation. Furthermore, the increments for the dipolar and chemical shift evolutions need not be the same: because the ^{1}H chemical shift signal decays faster than the dipolar signal, the number of MREV-8 cycles in each chemical shift increment was chosen to be smaller than the number in each dipolar coupling increment. This results in a combined PDLF and ^{1}H chemical shift dimension in which the dwell times,

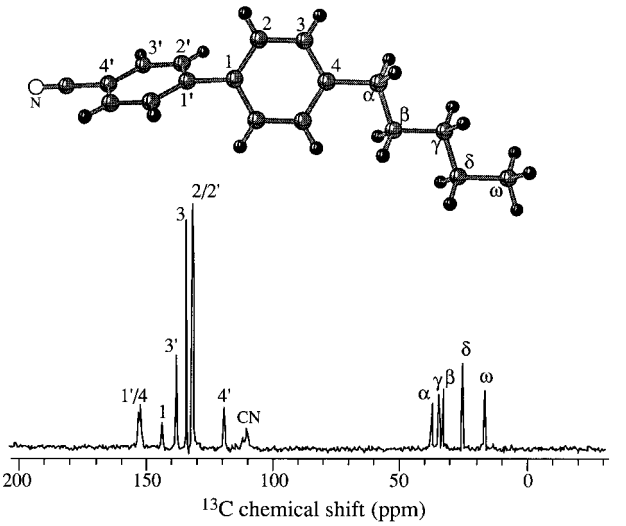

Figure 2. Chemical structure of 5CB and its 1D ^{13}C CP spectrum, obtained under sample spinning about an axis inclined at 50.7° to the magnetic field. Except for C2 and C2′ sites, all carbon sites are resolved at this angle.

or the spectral widths, of the two subdimensions differ by an integer ratio *n*. The variability of the relative dwell times makes it possible to enhance preferentially the resolution associated with one of the two interactions.

Results and Discussion

C−H Dipolar Couplings by PDLF Spectroscopy. The chemical structure of 5CB (Figure 2) consists of an *n*-pentyl chain attached to two aromatic rings, which are connected further to a nitrile group. The ^{13}C chemical shifts of most sites are well-resolved at the spinning angle of 50.7° and have been previously assigned,[10] as shown in Figure 2.

The 5CB PDLF spectrum, correlating C−H dipolar couplings with the ^{13}C chemical shift, is presented in Figure 3. Each ^{13}C cross section exhibits one or more doublets that are symmetric around the zero frequency in the center of the spectrum. Since the frequency scale of the C−H coupling dimension is corrected for the MREV-8 scaling factor but not for the spinning scaling factor, these doublet splittings correspond, to a first approximation, to the motionally averaged C−H dipolar couplings scaled by the spinning factor, $P_2(\cos 50.7°) = +0.102$. The largest splitting in each ^{13}C cross section results from the directly bonded C−H coupling. In the aliphatic region of the spectrum (Figure 3a), we observe an increase in the short-range C−H couplings from the chain end ω-methyl group to the α-methylene group closest to the phenyl rings, except for a size reversal between the β and γ segments. This trend reflects the increasing stiffness of the chain toward the more rigid aromatic core. In addition to the large splitting in each ^{13}C cross section, we observe smaller splittings in the Cδ (69 ± 17 Hz), Cα (69 ± 17 Hz), and Cγ (35 ± 17 Hz) slices and a broadening of the zero-frequency peak in the Cβ cross section. These small splittings or indications of small splittings result from the dipolar couplings between unbonded ^{13}C and ^{1}H spins and can be assigned tentatively by geometric arguments. For example, the small C−H splitting in the Cδ cross section may result from either the Cδ−Hω coupling or the Cδ−Hγ coupling. Although no small splitting is observed in the Cω cross section, a zero-frequency peak is found that originates from unresolved long-range C−H dipolar couplings. This zero-frequency peak is relatively sharp and has lower intensity compared to the broader and more intense zero-frequency peaks in other carbon slices. This can be attributed to the additional motional averaging by the three-site jumps of the Cω-methyl group. Note that, in contrast to the PDLF spectrum, the zero-frequency region of a carbon-detected SLF spectrum can be crowded with overlapping peaks due to the long-range dipolar couplings and the difference frequencies of nearly degenerate directly bonded dipolar couplings, thus resulting in lower resolution.

An exact analysis must account for the fact that the short-range C−H couplings in the PDLF spectrum have contributions from the scalar (*J*) coupling as well as the dipolar coupling. However, since the scalar coupling is isotropic and does not change with the spinning factor $P_2(\cos\theta)$, the two contributions can be separated by the measurement of several PDLF spectra at different spinning angles.[10,32] Only the anisotropic dipolar coupling scales with $P_2(\cos\theta)$, so that a linear fit of the observed splittings as a function of $P_2(\cos\theta)$ yields the C−H dipolar coupling as the slope of the line and the $^{1}J_{C-H}$ as the intercept. Results on the precise measurement of the short-range C−H dipolar couplings in 5CB will be described in a later paper.[33] For the time being, we concentrate on the long-range C−H dipolar couplings, which are determined here unambiguously for the first time. Their strengths correspond to the small splittings observed in the spectra. Adjustments for small $^{n}J_{C-H}$ ($n > 1$) couplings[34] are not made here because the multiple-bond *J* couplings are relatively small, and the signs of the C−H dipolar couplings relative to the *J* coupling, which are required for taking into account the *J* coupling in the observed splitting, cannot be determined from these spectra.

Shown in Figure 3b are the dipolar couplings of the aromatic sites. The directly bonded C−H couplings are generally smaller than the corresponding aliphatic ones, probably because the angles between the phenylene C−H bonds and the nematic director are closer to the magic angle. The most significant features in this part of the spectrum are the double splittings of the protonated C2/C2′, C3, and C3′ sites, where the smaller splitting, about 230 Hz, is approximately one-half of the larger splitting. Since each protonated phenylene carbon has only one directly bonded proton, the smaller splittings must result from long-range C−H couplings. On the basis of geometric considerations, these long-range couplings may be tentatively assigned to the proton of the neighboring carbon site on the same phenylene ring. For example, the small splitting in the C3 slice can be attributed to the C3−H2 dipolar coupling, whereas the small splitting in the C2/C2′ slice results from the C2−H3 and C2′−H3′ couplings. The coincidence of the C2 and C2′ chemical shifts makes it difficult to distinguish the C−H dipolar couplings of these two sites. The similarity in the short-range C−H couplings of different aromatic sites suggests conformations in which the C2−H2 and C2′−H2′ bonds, for example, form similar angles with the main symmetry axis of the nematic phase.

The presence of the long-range (specifically, two-bond) C−H dipolar couplings among the protonated aromatic sites was indicated previously on the basis of simulations of SLF spectra.[10] The long-range couplings obtained from the current PDLF data (Table 2) agree with their results. This consistency confirms the precision of the PDLF method. However, it is important to realize that the current PDLF experiment has the advantage that the long-range dipolar couplings can be read off directly from individual spectral splittings rather than by using indirect simulations.

The high resoluton of the PDLF technique is demonstrated further in the C−H spectra of the quaternary carbons C4 and C4′. Both sites exhibit a long-range C−H coupling of 140 ± 20 Hz, which is observed here for the first time. The splitting in the C4 cross section can be assigned to either the intra-

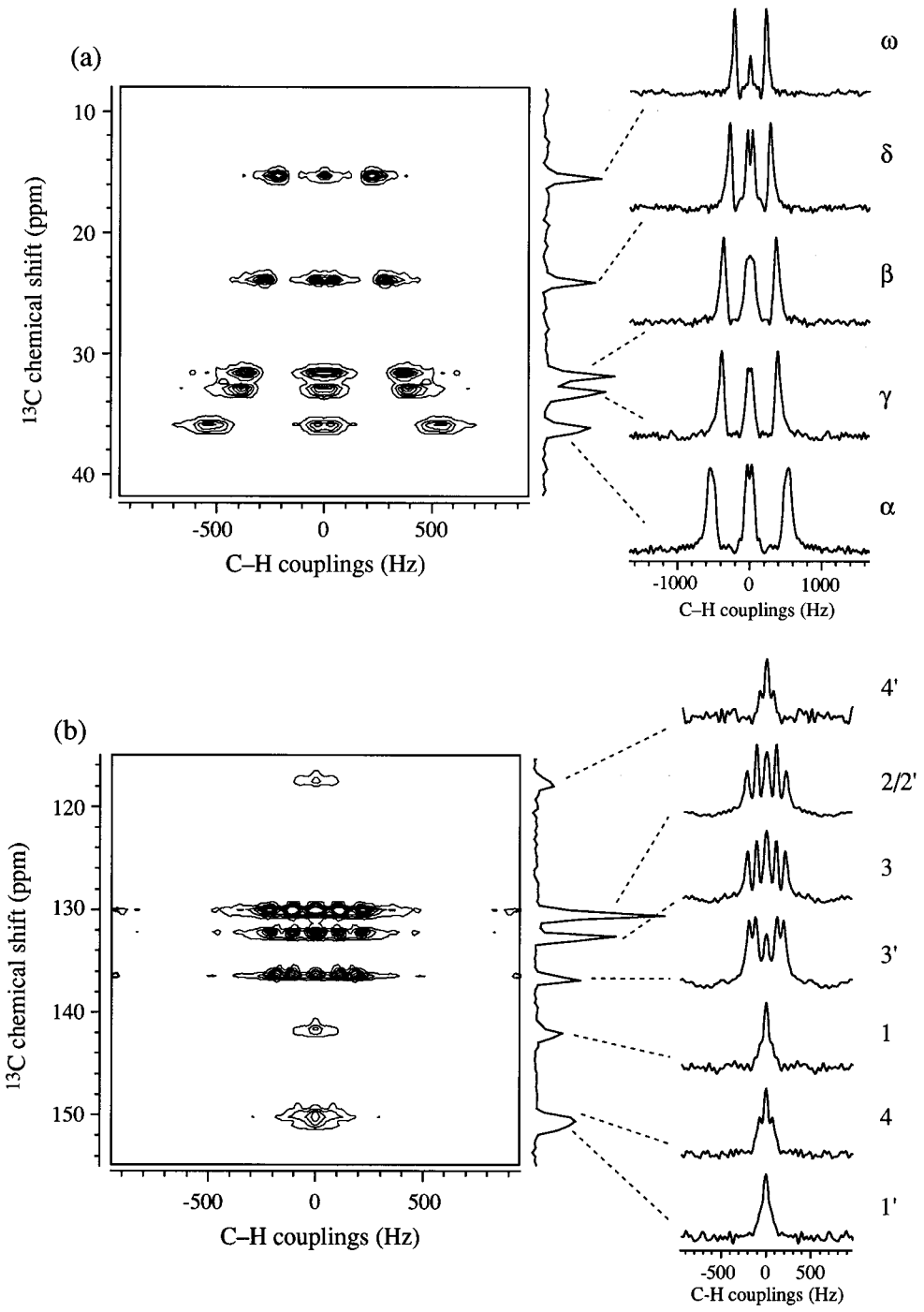

Figure 3. PDLF spectrum of 5CB. (a) Aliphatic region. The largest C−H dipolar coupling in each ^{13}C cross section increases from Cω to Cα, indicating increasing stiffness of the chain toward the phenylene rings. Long-range C−H dipolar couplings are resolved at Cδ, Cγ, and Cα sites. (b) Aromatic region. The C2/C2′, C3, and C3′ sites each exhibit two distinct C−H splittings, with the larger splitting being approximately twice the magnitude of the smaller one. The quaternary C4 and C4′ carbons exhibit long-range C−H dipolar couplings of about 140 Hz. The sample was spun about an axis inclined at 50.7° to the magnetic field at a rate of about 1.6 kHz. The spectrum was acquired in 15 h.

TABLE 2: Resolved and Assigned Long-Range C−H Dipolar Couplings (kHz) in 4-Pentyl-4′-biphenylcarbonitrile[a]

^{13}C	^{1}H	coupling	^{13}C	^{1}H	coupling
Cδ	Hω	0.36 ± 0.10	C3	Hα	0.54 ± 0.15
Cγ	Hβ	0.17 ± 0.10	C3	H2	1.12 ± 0.10
Cβ	Hδ/Hγ	0.30 ± 0.10	C2	H3	1.17 ± 0.10
Cα	Hβ	0.35 ± 0.12	C2′	H3′	1.17 ± 0.10
C4	Hα	0.76 ± 0.15	C3′	H2′	1.11 ± 0.10
			C4′	H3′	0.72 ± 0.10

[a] Only the absolute values are given since the sign cannot be determined from the experiments described.

aromatic C4−H3 coupling or the aromatic−aliphatic C4−Hα coupling, since the C4 carbon is located at the junction of the phenylene ring and the aliphatic chain so that both protons are two bonds away. In contrast, the coupling in the C4′ slice must be due to the H3′−C4′ coupling because the H3′ protons are closest to the quaternary C4′.

Qualitative C−H Dipolar Couplings by HETCOR Spectroscopy. The observed long-range C−H dipolar couplings and their assignments can be confirmed by a HETCOR experiment that correlates the ^{13}C and ^{1}H chemical shifts. Because the ^{13}C magnetization is transferred from ^{1}H by cross polarization, a peak in the correlation spectrum indicates the presence of a specific C−H dipolar coupling. Shown in Figure 4 is the HETCOR spectrum of 5CB, obtained with 3 ms of mixing time for ^{1}H spin diffusion and 2.5 ms of CP contact time. In the

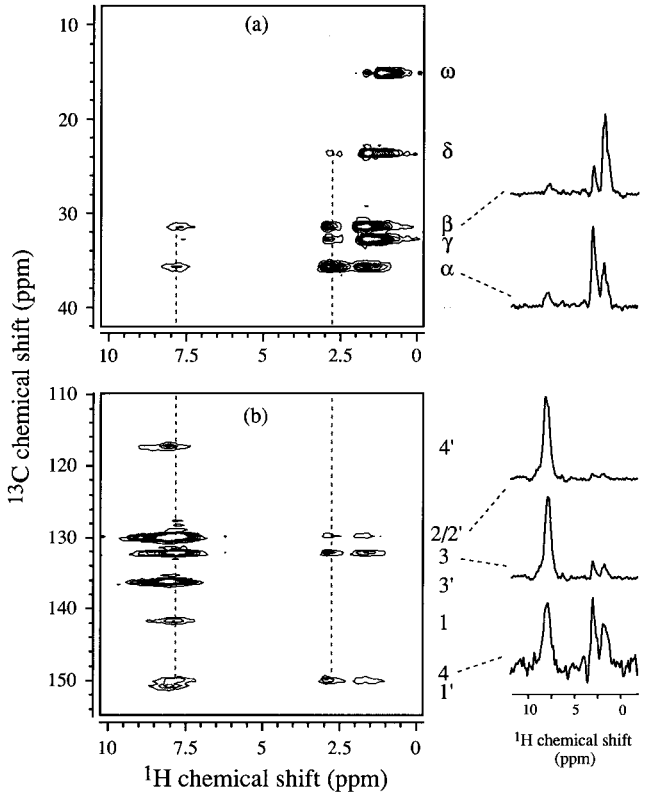

Figure 4. ^{13}C−^{1}H chemical shift correlation spectrum of 5CB. (a) Aliphatic region. Cross peaks due to long-range Cα−Hβ, Cγ−Hα, and Cβ−Hα dipolar couplings can be clearly observed. Cα and Cβ also couple to the aromatic H3 and H2 protons, as shown by the low-intensity peaks above 7.5 ppm. (b) Aromatic region. Cross peaks due to long-range Ci−Hα and Ci−Hβ (i = 2−4) dipolar couplings can be observed at the respective frequencies. The dashed lines guide the eyes for the H3/2 and Hα chemical shifts. The ^{1}H mixing time and CP contact time were 3 and 2.5 ms, respectively. The spinning angle was 50.7°. The spectrum was acquired in 18 h.

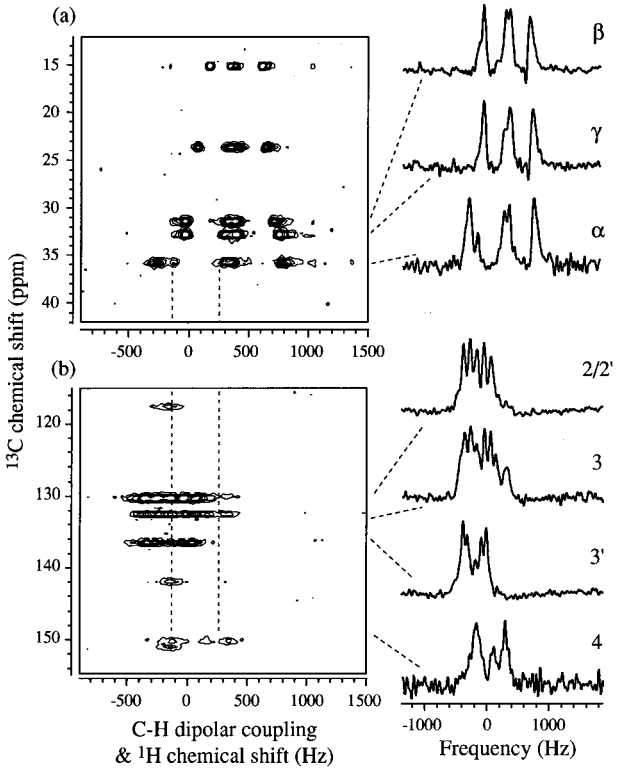

Figure 5. Reduced-3D spectrum of 5CB, obtained with a ^{1}H PDLF:CS dwell time ratio (n) of 4. (a) Aliphatic region. The small C−H splittings at the Cα and Cβ sites are assigned to the Cα−Hβ and Cβ−Hδ couplings on the basis of the ^{1}H chemical shift. An incompletely resolved Cα−H3 coupling can also be seen in the Cα slice. (b) Aromatic region. In addition to intra-aromatic long-range couplings such as the C3−H2 coupling, dipolar couplings between aromatic carbons and aliphatic protons are observed. The C3−Hα splitting is about 120 Hz. The quaternary C4 carbon shows significant couplings to both the H3/H2 proton and the aliphatic Hα proton (180 ± 30 Hz). The left and right dashed lines in the spectra correspond to the H3/H2 and Hα chemical shifts, respectively. The spinning angle was 50.7°. The measuring time was 15.5 h.

aliphatic ^{13}C chemical shift region (Figure 4a), the ^{1}H chemical shifts for the Hβ, Hγ, and Hδ protons are essentially indistinguishable, whereas the Hω and Hα protons exhibit different chemical shifts. In addition to the resonances from the directly bonded C−H pairs, cross peaks due to the unbonded C−H pairs are also seen. For example, signals due to the Cβ−Hα, Cγ−Hα, Cγ−Hβ, and Cα−Hβ couplings are observed at the respective ^{13}C and ^{1}H chemical shifts. In addition to these intra-aliphatic C−H dipolar couplings, aliphatic and aromatic C−H couplings can also be observed. For example, the cross peaks above 7.5 ppm in the Cα and Cβ slices result from the Ci−H3 and Ci−H2 couplings (i = α, β). The possibility that the H2′ and H3′ protons are coupled significantly to these aliphatic carbons can be ruled out, not only because of the large internuclear distances between the aliphatic carbons and the Hi′ (i = 1−4) protons but also because the chemical shifts of the protons on the two phenylene rings can be resolved. Judging from the small but discernible chemical shift difference between the H3′ and H3 protons, the Cα and Cβ carbons couple with the H2 and H3 protons, whose chemical shifts are more upfield than those of the H2′ and H3′ protons.

The aromatic region of the HETCOR spectrum (Figure 4b) confirms the existence of the aliphatic and aromatic C−H dipolar couplings. In the C2/C2′ and C3 slices, cross peaks are observed at the Hα and Hβ chemical shifts, and the peak intensities are stronger in the C3 slice than in the C2/C2′ slice. This intensity difference is consistent with the closer distance of the C3 carbon to the aliphatic chain. Furthermore, the quaternary carbon C4 exhibits strong peaks at the H2/H3, Hα, and Hβ chemical shifts. This indicates the presence of significant C4−Hα and C4−Hβ dipolar couplings, which cannot be observed in other parts of the spectrum. In comparison, the quaternary C1, C1′, and C4′ carbons, which are farther away from the aliphatic chain, exhibit resonances only at the chemical shifts of the phenylene ring protons.

Quantitative Assignment of Long-Range C−H Dipolar Couplings. The analysis so far has shown that the PDLF technique resolves long-range C−H dipolar couplings, whereas the HETCOR experiment identifies the coupling partners. It would be natural to combine these two techniques into a single experiment that correlates the C−H dipolar couplings, the ^{1}H chemical shifts, and the ^{13}C chemical shifts. Such a 3D experiment would require processing and storage of large data sets because both the PDLF and the ^{13}C chemical shift dimensions require long acquisition times to resolve the small dipolar couplings as well as the sharp resonance lines typical of motionally averaged systems. The difficulties of this full-3D experiment can be circumvented by the reduced-3D experiment described in the Experimental Section.

Figure 5 displays the reduced-3D spectrum of 5CB, acquired with a ^{1}H PDLF:CS dwell time ratio (n) of 4. The frequencies of the horizontal axis refer to the C−H dipolar couplings, so that the chemical shift frequencies are 4 times larger. The zero frequency of the axis corresponds to the ^{1}H carrier frequency and is not referenced to a chemical shift standard. Several C−H splittings, displaced according to the ^{1}H chemical shift, are observed in each ^{13}C cross section. The center of the largest splitting corresponds to the chemical shift of the directly bonded

proton, whereas the centers of the smaller splittings reveal the chemical shifts and therefore the identities of the unbonded protons that are coupled to the same carbon.

In the aliphatic region of the spectrum (Figure 5a), long-range Cα−Hβ and Cα−H3 dipolar couplings can be identified. Because the Hα chemical shift is well-separated from others, the center of directly bonded Cα−Hα coupling does not overlap with those of the long-range Cα−H splittings. The Cα−Hβ coupling is manifested as a splitting of 74 ± 17 Hz centered about +342 Hz, which is also found to be the center of the Cβ−Hβ doublet in the Cβ cross section. This measured value of Cα−Hβ coupling is consistent with the result from the PDLF experiment and confirms the assignment by the HETCOR experiment. Because the Cα−Hγ distance is larger, the Cα−Hγ coupling is likely to be smaller and the corresponding doublet may be buried under the more intense Cα−Hβ peaks. In the Cα slice, we can also identify a peak with unresolved splitting at −124 Hz, which can be assigned to either the Cα−H3 or Cα−H2 coupling. A distinction between these two possibilities cannot be made on the basis of this experiment due to the similarity of the H2 and H3 chemical shifts at this spinning angle.

Due to the limited resolution of the dipolar dimension in the spectrum, quantitative determination of the Cα−H3 (or Cα−H2) coupling is not possible. In fact, the mixed dipolar shift dimension of the reduced-3D spectrum shows less resolved resonance peaks than the pure dipolar dimension in the PDLF spectrum. The time evolution corresponding to the combined frequency dimension is a product of two decaying signals:

$$F(t_1) = [f(\omega_{CS}t_1)\exp(-t_1/T_{2CS}^*)][f(n\omega_D t_1)\exp(-nt_1/T_{2D}^*)]$$

where T_{2CS}^* and T_{2D}^* are the decay constants of the chemical shift and dipolar coupling signals, respectively. The Fourier transform of this function with respect to t_1 is the convolution of the two contributions. For the case of an isolated C−H pair, the spectrum is a doublet centered at the ^{1}H chemical shift and has a FWHM of $(1/T_{2CS}^* + n/T_{2D}^*)/\pi$ Hz. Since the 180° pulse in the PDLF evolution refocuses field inhomogeneities in addition to chemical shifts, $T_{2D}^* > T_{2CS}^*$. Thus, the best resolution in the mixed frequency dimension of the reduced-3D spectrum is achieved when the chemical shift line shape acts as a matched filter for the dipolar signal, i.e., when $T_{2CS}^* = T_{2D}^*/n$. This effect is demonstrated, for example, by the higher resolution of the Cβ cross section with $n = 4$ (Figure 5) than with $n = 2$ (Figure 6).

Note that the lack of resolved long-range couplings in the PDLF spectrum does not necessarily indicate the resolution limit of the reduced-3D spectrum. In the PDLF spectrum, all C−H couplings of a ^{13}C site are centered at the zero frequency, so that the zero-frequency peak can be the superposition of several long-range C−H couplings. In the reduced-3D experiment, however, these small long-range dipolar couplings are displaced according to the ^{1}H chemical shifts so that enhanced resolution is possible. The Cβ cross section in Figures 3a and 5a demonstrates such a resolution difference.

Figure 5b shows the aromatic ^{13}C region of the same reduced-3D spectrum. We observe intra-aromatic C−H couplings, which are barely shifted from the directly bonded C−H couplings due to the nearly identical chemical shifts of the aromatic protons at this spinning angle. Dipolar couplings between the aliphatic protons and the aromatic carbons can be identified more clearly. For example, the C3−Hα coupling can be assigned: the left peak of the splitting is displayed as a shoulder of the main signals at 173 Hz, the right peak is located at 297 Hz, and the center of the two matches the Hα chemical shift. On the basis of this assignment, the C3−Hα coupling is

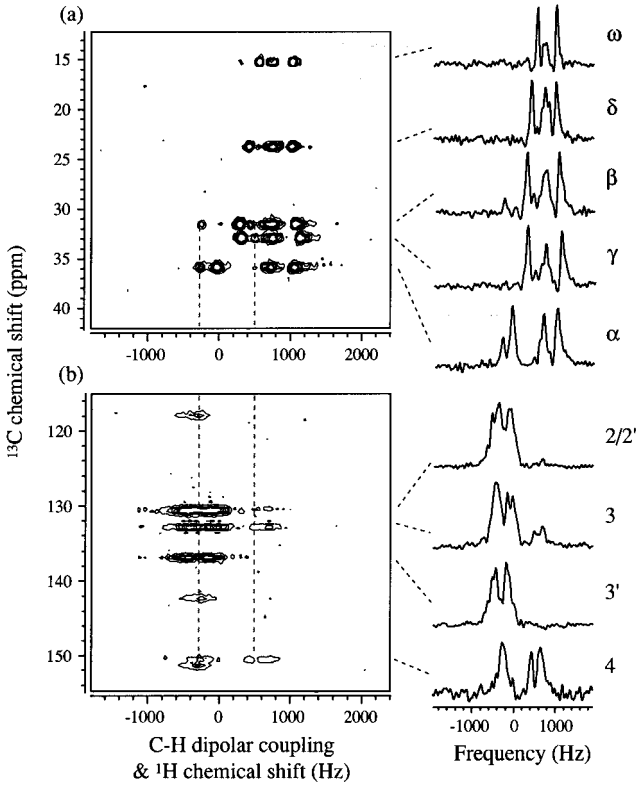

Figure 6. Reduced-3D spectrum of 5CB, taken with a ^{1}H PDLF:CS dwell time ratio (n) of 2. (a) Aliphatic region. Several long-range couplings, such as Cα−Hβ and Cδ−Hω couplings, are resolved. (b) Aromatic region. The C3−Hα and C4−Hα couplings can be identified clearly. The long-range C−H splittings are more displaced from the centers of the directly bonded C−H splittings than in Figure 5 as a result of the reduced ^{1}H chemical shift spectral width. The left and right dashed lines in the spectra correspond to the H3/H2 and Hα chemical shifts, respectively. The spinning angle was 50.7°. The spectrum was measured in 19 h.

determined as 120 ± 30 Hz. In comparison, the C3′ cross section exhibits no cross peaks in the aliphatic ^{1}H chemical shift region, which is consistent with the larger distance of the C3′ carbon to the aliphatic chain. The C4 slice exhibits unresolved signals at the H2/H3 chemical shift as well as an asymmetric doublet at the Hα chemical shift. The magnitude of the C4−Hα coupling is 180 ± 30 Hz, which is consistent with the PDLF result within the error margin. Overall, the spectra shown here indicate that the C4 carbon couples more strongly to the aliphatic Hα proton than to the aromatic protons.

To confirm the assignment of the long-range C−H dipolar couplings, we performed a second reduced-3D experiment with a ^{1}H PDLF:CS dwell time ratio (n) of 2, keeping the chemical shift dwell time the same as before. This causes a contraction of the spectral width of the ^{1}H chemical shift relative to that of the dipolar coupling and results in an increased separation of the C−H doublets in each ^{13}C cross section. Figure 6 exhibits the reduced-3D spectrum with $n = 2$. In the Cα slice (Figure 6a), the high-intensity signal at 725 Hz coincides with the chemical shifts of Hβ or Hγ and is clearly shifted from the center of the large doublet with a splitting of 1.08 kHz. Furthermore, the dipolar coupling of Cα to the aromatic H3 or H2 protons is manifested as an unsplit peak at −264 Hz. In the aromatic ^{13}C region (Figure 6b), the C3 cross section exhibits a C3−Hα dipolar coupling of 100 ± 25 Hz, which is consistent with the value obtained from Figure 5. However, due to the reduced dwell time of the dipolar evolution, the resolution of the C−H couplings is lower than that of the previous spectrum, and many long-range C−H dipolar couplings cannot be measured precisely.

Table 2 summarizes the long-range C−H dipolar couplings in 5CB that are measured and assigned by the PDLF, HETCOR, and reduced-3D experiments. The dipolar coupling strengths are calculated as the average of the values from Figures 3, 5, and 6 and are weighted according to the resolution of each spectrum. The convention of defining half of a splitting as the dipolar coupling is followed. Since the signs of these long-range couplings cannot be obtained from the current spectra, only the absolute values of the couplings are listed.

Further improvements in the resolution of the present experiments can be achieved by changing the spinning angle to values that correspond to larger scaling factors. A factor of 3 or 4 in $P_2(\cos\theta)$ can be conveniently gained if the rotor axis is inclined at 43° or 39° to the magnetic field. Unfortunately, there are drawbacks associated with setting the spinning axis at smaller angles. First, because the rf coil is wrapped around the stator in our VAS probehead,[23] the effective rf power is reduced when the stator axis is aligned more closely with the magnetic field. Consequently, MREV-8 decoupling will be less efficient, resulting in a loss of spectral resolution. In addition, the dipolar Hamiltonian parameters become larger at spinning angles farther away from the magic angle. In principle, the best-resolved dipolar couplings could be obtained from a static sample that has a scaling factor of either 1 or 0.5, depending on whether the nematic director is parallel or perpendicular to the magnetic field. However, the additional degree of freedom due to spinning allows delicate control of the experimental conditions, such as the maximum rf power and the largest detectable frequency. The latter is also a function of the pulse length, as the dwell time of the indirect dimension is constrained to be a multiple of the MREV-8 cycle time.

Conclusion

A class of NMR techniques has been demonstrated that allows the detection and assignment of weak long-range C−H dipolar couplings in liquid crystalline phases that can orient along the rotor axis when spun in a magnetic field. The measurement relies on the high resolution achieved in PDLF experiments and incorporates polarization transfer over large distances. A $^{13}C-^{1}H$ chemical shift correlation experiment aids the assignment of the dipolar coupling partners. Simultaneous measurement and assignment of the long-range dipolar couplings are achieved in a novel reduced-3D experiment, in which the evolution periods of the C−H couplings and the ^{1}H chemical shifts are incremented simultaneously. This makes it possible to combine and scale two interactions in one spectral dimension to facilitate the resonance assignment and enhance the spectral resolution. Complete information on the long-range C−H dipolar couplings will be obtained by a full-3D experiment in which the dipolar coupling and the ^{1}H chemical shift interactions are detected independently. The techniques demonstrated here constitute methodologies that are complementary to the traditional SLF techniques and are expected to be useful in the investigation of the structure and order of many complex liquid crystalline systems.

Acknowledgment. This work is supported by the Director, Office of Energy Research, Office of Basic Energy Sciences, Materials Sciences Division of the U.S. Department of Energy, under Contract No. DE-AC03-76SF00098. We thank Professor K. Schmidt-Rohr for many valuable discussions about this work.

References and Notes

(1) Chandrasekhar, S. *Liquid Crystals*; Cambridge University Press: Cambridge, UK, 1992.
(2) *Nuclear Magnetic Resonance of Liquid Crystals*; Emsley, J. W., Ed.; D. Reidel Publishing: Dordrecht, The Netherlands, 1985.
(3) Photinos, D. J.; Samulski, E. T.; Toriumi, H. *J. Phys. Chem.* **1990**, *94*, 4688.
(4) *NMR Spectroscopy using Liquid Crystal Solvents*; Emsley, J. W., Lindon, J. C., Eds.; Pergamon Press: Aylesbury, 1975.
(5) Ter Beek, L. C.; Zimmerman, D. S.; Burnell, E. E. *Mol. Phys.* **1993**, *80*, 177.
(6) van der Est, A. J.; Kok, M. Y.; Burnell, E. E. *Mol. Phys.* **1987**, *60*, 397.
(7) Hester, R. K.; Ackermann, J. L.; Neff, B. L.; Waugh, J. S. *Phys. Rev. Lett.* **1976**, *36*, 1081.
(8) Opella, S. J.; Waugh, J. S. *J. Chem. Phys.* **1977**, *66*, 4919.
(9) Fung, B. M.; Afzal, J. *J. Am. Chem. Soc.* **1986**, *108*, 1107.
(10) Fung, B. M.; Afzal, J.; Foss, T. L.; Chau, M. *J. Chem. Phys.* **1986**, *85*, 4808.
(11) Courtieu, J.; Alderman, D. W.; Grant, D. M.; Bayles, J. P. *J. Chem. Phys.* **1982**, *77*, 723.
(12) Courtieu, J.; Bayle, J. P.; Fung, B. M. *Prog. NMR Spectrosc.* **1994**, *26*, 141.
(13) Weitekamp, D. P.; Garbow, J. R.; Pines, A. *J. Chem. Phys.* **1982**, *77*, 2870.
(14) Caravatti, P.; Bodenhausen, G.; Ernst, R. R. *Chem. Phys. Lett.* **1982**, *89*, 363.
(15) Nakai, T.; Terao, T. *Magn. Reson. Chem.* **1992**, *30*, 42.
(16) Schmidt-Rohr, K.; Nanz, D.; Emsley, L.; Pines, A. *J. Phys. Chem* **1994**, *98*, 6668.
(17) Caravatti, P.; Braunschweiler, L.; Ernst, R. R. *Chem. Phys. Lett.* **1983**, *100*, 305.
(18) Roberts, J. E.; Vega, S.; Griffin, R. G. *J. Am. Chem. Soc.* **1984**, *106*, 2506.
(19) Emsley, J. W.; Luckhurst, G. R.; Stockley, C. P. *Mol. Phys.* **1981**, *44*, 565.
(20) Emsley, J. W.; Luckhurst, G. R.; Gray, G. W.; Mosley, A. *Mol. Phys.* **1978**, *35*, 1499.
(21) Sinton, S. W.; Zax, D. B.; Murdoch, J. B.; Pines, A. *Mol. Phys.* **1984**, *53*, 333.
(22) Guo, W.; Fung, B. M. *J. Chem. Phys.* **1991**, *95*, 3917.
(23) Eastman, M. A.; Grandinetti, P. J.; Lee, Y. K.; Pines, A. *J. Magn. Reson* **1992**, *98*, 333.
(24) Mansfield, P. *J. Phys. Chem.* **1971**, *4*, 1444.
(25) Rhim, W.-K.; Elleman, D. D.; Vaughan, R. W. *J. Chem. Phys.* **1973**, *59*, 1740.
(26) Hartman, S. R.; Hahn, E. L. *Phys. Rev.* **1962**, *128*, 2042.
(27) Pines, A.; Gibby, M. G.; Waugh, J. S. *J. Chem. Phys.* **1973**, *59*, 569.
(28) States, D. J.; Haberkorn, R. A.; Ruben, D. J. *J. Magn. Reson.* **1982**, *48*, 286.
(29) Caravatti, P.; Neuenschwander, P.; Ernst, R. R. *Macromolecules* **1985**, *18*, 119.
(30) Bodenhausen, G.; Ernst, R. R. *J. Magn. Reson.* **1981**, *45*, 367.
(31) Bodenhausen, G.; Ernst, R. R. *J. Am. Chem. Soc.* **1982**, *104*, 1304.
(32) Hong, M.; Schmidt-Rohr, K.; Pines, A. *J. Am. Chem. Soc.* **1995**, *117*, 3310.
(33) Caldarelli, S., Hong, M., Emsley, L., Pines, A. Manuscript in preparation, 1996.
(34) Jameson, C. J. J Couplings. In *Multinuclear NMR*; Mason, J., Ed.; Plenum Press: New York, 1987; p 89.

JP960972M